LATIN AMERICAN JOURNAL OF SEDIMENTOLOGY AND BASIN ANALYSIS | VOL. 12 (1) 2005, 3-21
(C) Asociación Argentina de Sedimentología - ISSN 1669 7316

MORPHOLOGY AND FORMATION OF GLASSY VOLCANIC ASH FROM THE AUGUST 12-15, 1991 ERUPTION OF HUDSON VOLCANO, CHILE

Roberto A. SCASSO [1] *and Steven CAREY* [2]

[1]Departamento de Ciencias Geológicas, Facultad de Ciencias Exactas y Naturales, Universidad de Buenos Aires, Ciudad Universitaria, Pabellón 2. Buenos Aires, Argentina. E-mail: rscasso@gl.fcen.uba.ar
[2]Graduate School of Oceanography, University of Rhode Island, Narragansett R.I., USA

Abstract: The 1991 explosive eruption of Hudson volcano in Chile ejected about 2.7 km^3 (DRE) of basalt and trachyandesite magma as tephra fall. A majority of the fallout occurred from an eruption during the period August 12-15, 1991, producing an extensive deposit to the east of the volcano in Chile and Argentina. Dacitic, glassy tephra from this phase of the eruption exhibit a remarkable variety in particle morphology and color, ranging from dark, poorly-vesicular shards to light-colored, pipe-vesicular micropumice. Fractal analysis of glassy particle outlines shows that at least four distinct types can be discriminated: blocky, poorly-vesicular, highly vesicular with spherical vesicles, and pipe vesicular. A quantitative comparison of particle morphologies using principal component analysis of fractal spectrums of the Hudson tephra with other tephra produced by eruptions with known fragmentation mechanisms, together with SEM imaging of particle surfaces, indicates that production of the Hudson tephra involved both interaction with external water and exsolution of dissolved volatiles. Blocky particles likely represent magma that was fragmented by magma-water interactions before exsolution of all dissolved volatiles could occur. The great diversity of particle types in the August 12-15, 1991 Hudson tephra fall can be attributed to eruption of volatile-rich trachyandesite magma through an ice-filled caldera where subglacial melting led to a supply of external water that interacted intermittently with the discharge of magma driven primarily by volatile exsolution.

Resumen: La erupción explosiva de 1991 del Volcán Hudson en Chile expulsó cerca de 2,7 km^3 (DRE) de magma traquiandesítico y basáltico en forma de caída de tefra. La mayoría de la caída se produjo durante el periodo del 12 al 15 de agosto de 1991, a partir de una erupción que produjo un extenso depósito hacia el este del volcán, en Chile y en Argentina. Para esta fase de la erupción, la fracción vítrea correspondiente a la tefra traquiandesítica muestra composición dacítica, con fragmentos de forma y color muy variados, que fluctúan desde trizas oscuros y poco vesiculadas hasta fragmentos pumíceos de color claro e intensa vesiculación de canalículos. El análisis fractal del contorno de las partículas vítreas permite la separación en por lo menos cuatro tipos distintos: blocosas, poco vesiculadas, altamente vesiculadas con vesículas esféricas y canalículo-vesiculadas. El análisis cuantitativo de las formas de las partículas, mediante el análisis de componentes principales de los espectros fractales de las partículas de la tefra del Hudson, y su comparación con los de otras tefras producidas por erupciones cuyos mecanismos de fragmentación son conocidos, junto con las imágenes de microscopio electrónico de barrido de la superficies de las partículas, indica que la producción de tefra del Hudson es resultado de un proceso mixto que comprende la interacción del magma con agua externa y la exsolución de los volátiles disueltos en el magma. Las partículas blocosas probablemente representan magma fragmentado por interacción con agua antes de que tuviera lugar la exsolución de todos los volátiles disueltos. La gran variedad de partículas en la caída de cenizas de la erupción del 12 al 15 de agosto de 1991 del volcán Hudson puede

atribuirse a la erupción de un magma traquiandesítico rico en volátiles a través de una caldera rellena de hielo, en la cual la fusión de la base del relleno de hielo aportó agua externa al sistema magmático, que interactuó intermitentemente con la descarga de magma impulsada por la exsolución de volátiles.

Keywords: Hudson Volcano, Patagonia, 1991 eruption, explosive eruption, fractal analysis, particle morphology, glass, ash.
Palabras clave: Volcán Hudson, Patagonia, erupción de 1991, erupción explosiva, análisis fractal, forma de las partículas, vidrio, ceniza.

INTRODUCCION

The morphology of tephra from explosive eruptions is controlled by a complex array of factors including magma composition, volatile content, eruptive process, and the influence of external water (Heiken and Wohletz, 1985; 1991). Some of these factors impart characteristic features on particle morphology and provide the means for interpreting eruptive processes from the study of ancient tephra deposits (e.g. Dellino and LaVolpe, 1996). In particular, the role of external water in the fragmentation process of explosive eruptions is often inferred from the morphological characteristics of tephra (*e.g.*, Wohletz, 1983). Hudson Volcano, located in the southern Andes of Chile (45°54¢S, 72°58¢W), had a paroxysmal, plinian (phreato-plinian?) eruption on 12-15 August 1991, which produced a land-based tephra volume of 4.4 km^3 (2.75 km^3 total DRE). Tephra was transported east-south-eastward by strong winds, and accumulated in a large, fan-shaped area of Patagonia, in Argentina and Chile (Scasso *et al.,* 1994). One of the striking features of this fall deposit is the great diversity of glass particle morphologies and color produced by this single eruptive event. Juvenile ash particles vary between dark-brown, non-vesicular blocky shards to whitish, highly-vesicular micropumice (Bitschene and Fernandez ,1995). The Hudson event thus provides an interesting example of varied types of magma vesiculation and fragmentation in a single eruption, allowing insights into the factors that control the shape of the particles, such as primary degassing, magma composition, rates of degassing and influence of external water.

In this paper we present the results of a quantitative analysis of tephra particle morphologies from the paroxysmal 1991 eruption of Hudson volcano. Fractal analysis is used to relate potential fragmentation mechanisms to specific particle shapes. In particular, morphologies of the Hudson particles are quantitatively compared with juvenile glassy particles from a variety of explosive eruptions with known fragmentation mechanisms through the use of principal component analysis. The results suggest that the diversity of particle morphologies was produced by eruption of volatile-rich trachyandesite magma that fragmented by a combination of both primary degassing and explosive interaction with external water.

GEOLOGICAL SETTING

Hudson volcano is located about 300 km to the east of the Nazca-Antarctic-South American plate triple junction, where the Chile Rise enters the Chile Trench (Naranjo and Stern, 1998). It is the southernmost volcano in the Andean southern volcanic zone (33°-46°S) and is built overlying Cretaceous granitic rocks from the Batolito Patagónico, a large plutonic unit along the axis of the Cordillera Patagónica (Fig. 1). Hudson Volcano covers an area of 300 km^2 and its summit is a 10-km-diameter, ice-filled caldera, whose southern wall rises to a height of 1905 m (Fig. 2). Naranjo and Stern (1998) estimated a glacial ice volume of 2.5 km^3 in the caldera, which drains to the northwest along the Huemules glacier. In spite of its intense Holocene-Recent activity, Mount Hudson was only recently recognized as a volcanic edifice by Fuenzalida and Espinosa (1974).

Holocene-Recent Explosive Activity of the Mount Hudson

Activity of the Hudson volcano started at about 1.0 Ma (Orihashi *et al.*, 2004) and the Holocene-Recent stratigraphy of its fall deposits record at least 12 explosive eruptions, with the most important being the August, 1991 eruption, and two others dated at approximately 3600 and 6700 BP (Naranjo and Stern, 1998). The 6700 yBP event is considered the largest

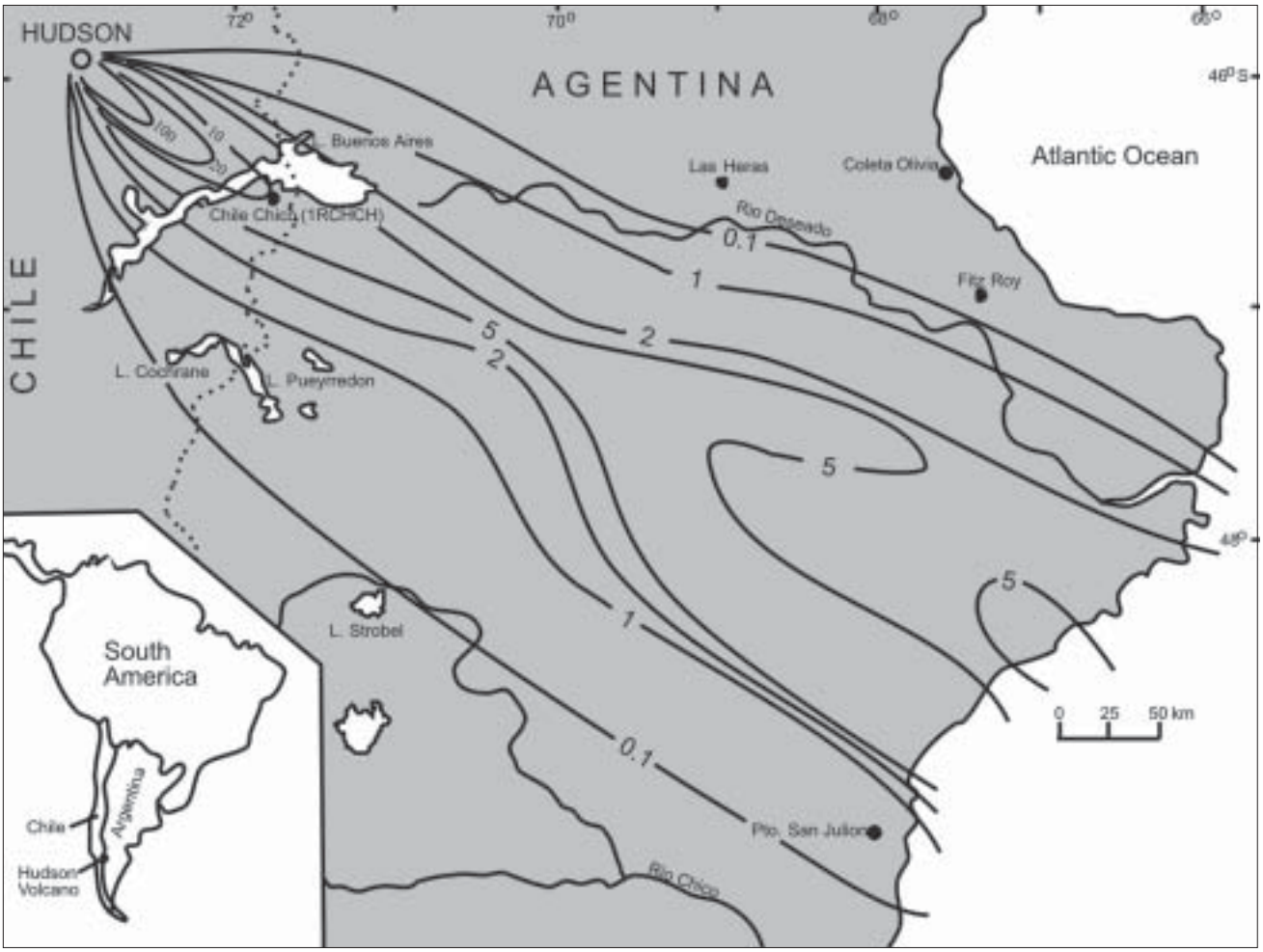

Figure 1. Distribution and thickness of tephra fall from the August 12-15, 1991 explosive eruption of Hudson volcano, Chile. Isopach thicknesses are in centimeters from Scasso *et al.* (1994). Location of the sample studied for the fractal analysis is shown at Chile Chico (1RCHCH). Inset map shows the location of Hudson volcano.

Figura 1. Espesor y distribución de la tefra de caída de la erupción explosiva del 12 al 15 de agosto de 1991 del Volcán Hudson, Chile. El valor de las isopacas, tomado de Scasso *et al.* (1994), es en centímetros. La muestra estudiada mediante análisis fractal corresponde a la localidad de Chile Chico (1RCHCH). El mapa inserto muestra la localización del Volcán Hudson.

for Hudson, and perhaps of any volcano in the southern Andes during the Holocene (Stern, 1991; Naranjo and Stern, 1998). Another historical eruption took place in August 1971, when a subplinian (phreatoplinian?) eruptive column rose to 14 km high. This event left a trachyandesitic tephra fall deposit (Fuenzalida, 1976) and triggered several lahars down the Huemules valley (Best, 1992). Bulk (trachyandesitic) and glass (dacitic) composition of the tephra is remarkably similar to that of the August 12-15, 1991 eruption.

August 1991 Eruption. Naranjo (1991) and Naranjo *et al.* (1993) presented a detailed description of the August 1991 eruption. It began on August 8 with a phreatomagmatic phase that produced a 12 km-high eruption column. Basaltic tephra fall was dispersed to the NNE, and considerable amounts of ash were deposited covering a N-S elongate area, up to 200 km north of the volcano (Banks and Iven, 1991). A 400 m wide crater was formed from the eruption and basaltic lava was extruded along a 4 km NNE oriented fissure. Shortly after the onset of the eruption the western front of the Huemules glacier burst and jökulhlaups flowed down the glacial valley.

After minor activity, the paroxsymal eruption commenced at about 12:00 Chile local time on August 12 and a densely loaded ash plume rose to at least 10 km height in the next two hours. At about 16:30 on August 13 the ash plume rose to 16 km, and at about 20:00 an eruption plume, extending 1200 km to the

southeast , became visible on AVHRR (NOAA 9 and 11) and GOES satellite images. The plume became disconnected from the volcano at about 12:00 on August 14 and continuous eruption began again at about 2000. On the morning of the August 15 the eruption ceased. By that time the plume had extended 1500 km southeast and at its widest point near the Malvinas Islands, it was 370 km wide. The 800 m wide crater of the second eruption was located within the caldera and 4.5 km to the southeast of the first crater (Fig. 2).

The August 12-15 tephra fall left a deposit covering approximately 100,000 km^2 (Corbella *et al.,* 1991a; b), about 60 cm thick 25 km to the SE of the volcano, where it consists of about twenty well-defined and laterally continuous beds up to coarse lapilli in size. Nine layers are present in Los Antiguos, 120 km east southeast from the vent (Scasso *et al.,* 1994, Figs. 2 and 3). These show rhythmic alternation of light grey, fine ash with grey beds rich in pumice up to 3 mm in size, and a high percentage of coarse ash. The three coarser-grained units are likely related to three main eruptive pulses probably associated with well-developed plinian eruptive columns, reflecting several events of increasing eruptive power separated by relatively calm periods as a result of partial vent closure. This mechanism has been suggested by Walker (1981) for multilayer deposits with alternating coarse and fine beds. The latter represent the fallout of residual fine ash from the eruption columns during periods of reduction of the eruption power. However, a change in the eruption style from plinian to phreatoplinian (*e.g.,* Walker, 1981) might also account for this sequence. The fine-grained layers are not co-ignimbrite ash falls (e.g. Criswell ,1987; Carey *et al.,* 1990) because the eruption did not produce pyroclastic flows.

One of the most striking features of the fall deposit from the paroxysmal event is its unusual thickness versus distance relationship. East-southeast from the volcano the thickness of the tephra fall decreases regularly from up to 250 cm (Banks and Iven, 1991) near the vent, to 8 cm at 120 km downwind, in Los Antiguos, close to Lake Buenos Aires (Fig. 1). Beyond this point the deposit has a very slight decrease in thickness up to the central area of Santa Cruz, 250 km east southeast from the vent, where it begins to thicken once again. A secondary thickness maximum is well developed at approximately 500 km from the vent. Many features of the August 12- 15, 1991 fall deposits are similar to those produced by Quizapu in 1932 (Hildreth and Drake, 1992) and Mount St. Helens in 1980 (Sarna-Wojicki *et al.,* 1982; Carey and Sigurdsson, 1982).

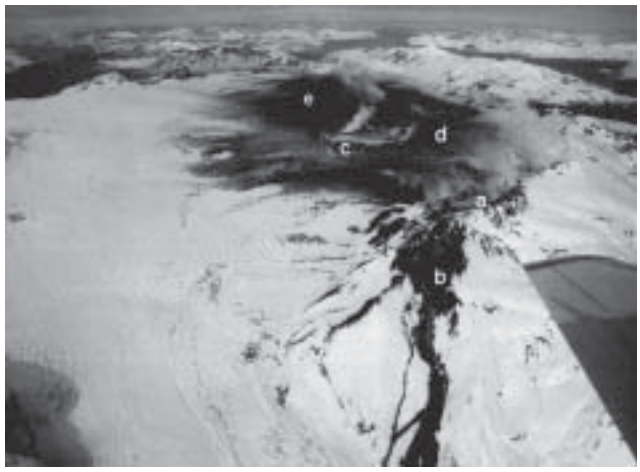

Figure 2. Aerial photograph of the Hudson caldera taken from the northwest on August 23, 1991. Basaltic dike from the August 8-10 eruption with intense fumarole activity (a) and lava flows to the northwest (b) Crater from the August 12- 15 eruption (c) bordered by a concentric pattern of ice crags (d). Dark material on the snow surface is tephra from minor explosive eruptions after August 20 (e). Photo courtesy of N.L. Banks.

Figura 2. Fotografía aérea de la caldera del Volcán Hudson, tomada desde el noroeste el 23 de agosto de 1991. El dique basáltico de la erupción del 8 al 10 de agosto muestra intensa actividad fumarólica (a) y una colada lávica que fluye hacia el noroeste (b). El cráter de la erupción del 12 al 15 de agosto (c) se encuentra rodeado por un enjambre concéntrico de grietas en el hielo (d). El material oscuro en la superficie de la nieve es tefra de una erupción menor ocurrida el 20 de agosto (e). Foto cortesía de N.L. Banks.

SAMPLES AND METHODOLOGY

Bulk samples of Hudson tephra deposited 100 km and up to 530 km from the vent were wet sieved and separated at 1 phi interval. Ten polished, uncovered thin sections of grain mounts were prepared for the size fractions between 0.125 and 0.250 mm. All the sections were studied under petrographic and binocular microscopes. As the general petrographic, and especially the glass characteristics, were similar in all the sections, a proximal and a distal sample were chosen for fractal analysis. A wide variety of glass particles showing different color, vesicularity and morphology is present in each sample. They were subdivided into four main types: blocky, low-vesicular, highly vesicular and pipe vesicular (Fig. 3) which are described in detail below. In addition, in order to compare the Hudson particles with those from other eruptions with inferred fragmentation styles the following samples were used: 3012-1246.2 (sideromelane shards from Pacific

seamount F, ~2000 m water depth (Batiza *et al.*, 1984)), TB-146 (a sample of the Tambora 1815 trachyandesite pumice fall collected on the island Sumbawa, Indonesia by S. Carey and H. Sigurdsson), SU-9620 (a sample of the phreatomagmatic tephra fall from the 1963-64 eruption of Surtsey volcano, Iceland collected by H. Sigurdsson), and ICE 95-042 (tephra fall from the subglacial 1918 eruption of Katla volcano, Iceland collected at Thakgil by S. Carey).

In order to perform fractal analysis, transmitted- and reflected-light digital photomicrographs of ten to fifteen selected particles of each type were collected. Reflected light images showed sharper outlines, thus providing better support for tracing the particle outlines. Binary black and white images were obtained by tracing the outline of the original image with a mouse, thresholding, and filling the traced outline using the Image 1.61 software of the National Institute of Health. All of the analyses in this study were performed on such traced outlines (see Carey *et al.,* 2000 and Maria and Carey, 2002 for a detailed discussion of the methodology applied here). Fractal analysis was performed by means of the dilation method devised by Flook (1978). It widens and smoothes an object's outline by replacing each pixel along its boundary with structural elements (approximating a circle) of increasingly larger size. For each increment of dilation, measurements of the diameter and the area of the dilated boundary are collected. The perimeter is calculated by dividing the area of the dilated boundary by its diameter. The fractal dimension is a function of this relationship, and is expressed on a Richardson plots (Richardson, 1961) of log (perimeter) vs log (dilation diameter) as equal to one minus the slope of the data. As the Richardson curves showed complex patterns, we applied the fractal spectrum technique, an alternative method of quantitatively analyzing dilation Richardson curves (Maria and Carey, 2002). It consists of calculating the first derivative of the dilation curve, producing a full spectrum of fractal dimensions over a range of scales, that are suitable input variables for multivariate statistical analysis. Principal component analysis was used to decompose the multivariate fractal spectrum data (correlation matrix) into smaller, manageable components (Morelli, 2002). The analytical technique was preset to determine 3 factors, component variables, for each particle. The original variables for each particle represent a system of data in multidimensional space. The factors are then plotted on binary plots of two factors for comparative purposes.

GENERAL TEPHRA CHARACTERISTICS

August 8 Eruption. The black, basaltic fallout ashes of the August 8 eruption are crystal-poor, vitric ashes composed of about 50% blocky to platy tachylite, 40-45% light-brown, highly vesicular, plagioclase-phyric sideromelane showing ragged morphology, 3-5% microlithic pyroclasts, and crystals of plagioclase, green clinopyroxene, and Fe-Ti oxide (Bitschene and Fernández, 1995). These deposits were attributed to an early phreato-Plinian phase of the 1991 eruption (Arias *et al.*, 1991; Nillni *et al.*, 1992; Bitschene *et al.*, 1992). They were deposited in an area to the northeast of the volcano and not intermingled with the tephra from the main August 12-15 event in the localities sampled for this study.

August 12-15 Eruption. Tephra from the main eruptive event is composed of glass shards, pumice fragments, crystals and lithic fragments of trachyandesite bulk composition. Grey to whitish-grey pumice fragments are the main component of the coarsest fraction, while glass shards are the dominant component of the finest fraction (< 0.062 mm), both showing dacitic composition. Pumiceous fragments have either thin, parallel tubular vesicles with a length/diameter ratio of about 15 or spherical vesicles.

In the Chile Chico and Los Antiguos area (100 to 120 km from the vent, Fig.1) coarse sand-sized pumices are equant to prolate and angular. Most pumice is light grey but there is a continuous color variation to dark brown or black. The dark pumice also grades into poorly vesicular glass with spheroidal vesicles and into blocky non-vesicular particles. The dark pumiceous clasts are commonly mixed with the grey pumice, but they tend to be concentrated in one particular stratigraphic horizon (Scasso *et al.,* 1994). Large, grey, pumice clasts with dark-colored patches have also been observed. Bitschene and Fernández (1995) described streaky banded pumice as mixtures of rhyolitic and trachyandesitic magmas, with the rhyolitic magma constituting less than 5% of the total magma volume. According to these authors, the denser and darker shards have slightly higher Mg, Ti , Fe and Ca, and lower silica contents than the lighter and clearer glass shards.

Fresh, subhedral to euhedral broken plagioclase, pyroxene, opaques and olivine, often with glass rinds, are the main crystal components. Glass shards always predominate in the fine mode (about 25 mm), where

the sum of the remaining components rarely exceed 5% of the total volume, and pumice dominate the coarse mode (Scasso *et al.,* 1994). The coarse mode shifts to smaller grain sizes and often merges into the fine mode with increasing distance from source. A concomitant rise in the percentage of shards within this coarse mode is observed as a function of distance form the volcano. Close to the source they are almost lacking, at 270 km they contribute about 33% of the volume, and at 450 km from the vent they make up about 50% of the coarse mode. Crystals compose up to 25 % of the total volume in the size fraction between 0.3 and 0.6 mm close to the volcano (Nillni *et al.,* 1992). At 120 km from the vent the crystal content decreases to 25% of the coarse mode (about phi 1.41 to phi 2.41 - 0.38 to 0.19 mm) and then rapidly decreases to only about 10% of the main mode beyond 270 km. Lithic fragments of andesite are more abundant in the size fraction greater than 0.6 mm (Mazzoni and Destéfano, 1992) and compose up to 20% of the coarser fraction at a locality 20 km from the volcano (Nillni *et al.,* 1992). However, lithic fragments are very scarce beyond 100 km from the vent, where juvenile fragments are the main components.

The proportions of particles in the fall deposit reflects both the original size of the components (e.g. crystals) in the magma as well as eolian fractionation due to the size, shape and density of the ejecta (Scasso *et al.,* 1994). As glass shards are pumice mainly broken during the eruption, they make an important contribution to the fine mode (about 0.015 mm). Fibrous pumice dominates this fraction due to the small diameter of the component vesicles. Bubble-wall cuspate and platy shards are the main components of the fine mode.

MORPHOLOGY OF GLASS ASH-SIZED PARTICLES

As described above, the 1991 Hudson fall deposits show a striking variety of glassy particles with different morphology, vesicularity, and color. Glass particles in the August 12-15 deposit were broadly grouped in four classes: blocky, low-vesicular, high-vesicular and pipe-vesicular (Figs. 3, 4). The blocky and low-vesicular particles are black to dark brown (they can be light brown under the petrographic microscope), whereas the high and pipe-vesicular are yellow to whitish-grey (colorless or almost colorless under the microscope). Blocky shards are equant in shape and their outlines are mainly the result of straight to slightly irregular or conchoidal fracture planes, sometimes present within the grains. However, as they grade to vesicular particles, many shards are fractured along the planes formed by large vesicles and vesicle trains. The vesicular particles, in turn, show a large variation in color and vesicularity, from low degrees of vesicularity to extremely high vesicularity. The former show generally equant shapes with irregular outlines, and are darker in color with rounded or elongate vesicles filled by clearer fine-grained material. The highly vesicular particles are also equant in shape but show a foamy texture with very irregular outlines. Big cavities produced by bubble coalescence are common and together with the normal size vesicles give the outlines a highly complex pattern with several orders of irregularity. The pipe-vesicular particles show silky texture and prolated-prismoidal form, with consistent rectangular to square sections. Sometimes these particles are twisted or bent along the «a» (longest) axis. Internally they display the characteristic fibrous texture resulting from abundant elongate vesicles, which control the fracture pattern. Thus, regular outlines can result from fracturing along the vesicles, but small-scale complex convolution is present in sections cut oblique or perpendicular to them. Different patterns of fragmentation are clearly related to the type of bubble, either spherical or elongate, within the particles. The former tend to result in isotropic fracturing and equant particles, whereas the latter mainly yields prolate particles with planes of rupture perpendicular and parallel to elongation. This becomes evident in the pipe-vesicular particles (Fig. 4) where the extremely elongate vesicles are very close one to the other. This results in a delicate pattern of small-scale irregularities in the outlines.

Each type of particle grades to the others. This is especially clear in the vesicular types. Rare particles with unusual characteristics, like dark blocky pipe-vesicular or mixed (two different types of glass in the same particle separated by a sharp contact), are also present.

Fractal Analysis of Particles

Fractal analysis has proven to be an effective technique for quantitatively defining the complexity of volcanic particle morphologies (Carey *et al.*, 2000; Carey *et al.*, 2001; Maria and Carey, 2002). We have applied these methods to particles from the Hudson fall deposit in order to investigate differences in morphology and to compare particles to well-documented examples of different fragmentation styles. The principal tool that

Figure 3. Examples of four major types of glassy ash particles from the August 12-15, 1991 Hudson eruption. a) blocky shards. b) low vesicular. **c**) highly vesicular, and d) pipe vesicular. Black and white bars are 100 microns in length.
Figura 3. Ejemplos de los cuatro tipos principales de partículas vítreas de ceniza del 12 al 15 de agosto de 1991; a) blocosas; b) pocos vesiculadas; c) altamente vesiculadas, y d) canalículo-vesiculadas. Las barras en blanco y negro tienen 100 micrones de largo.

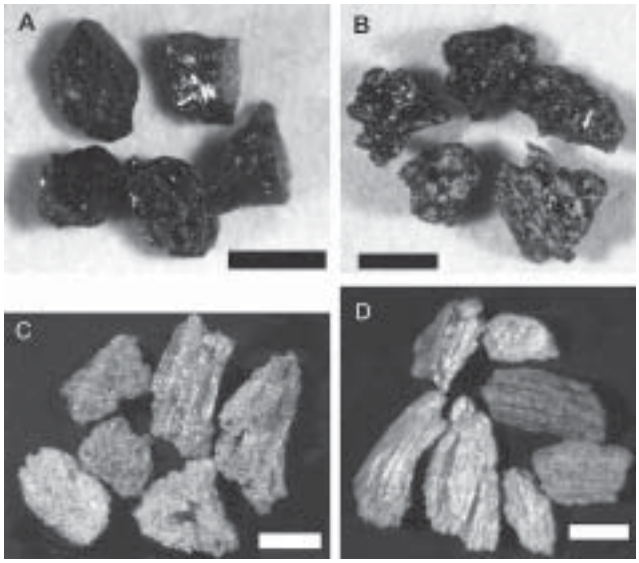

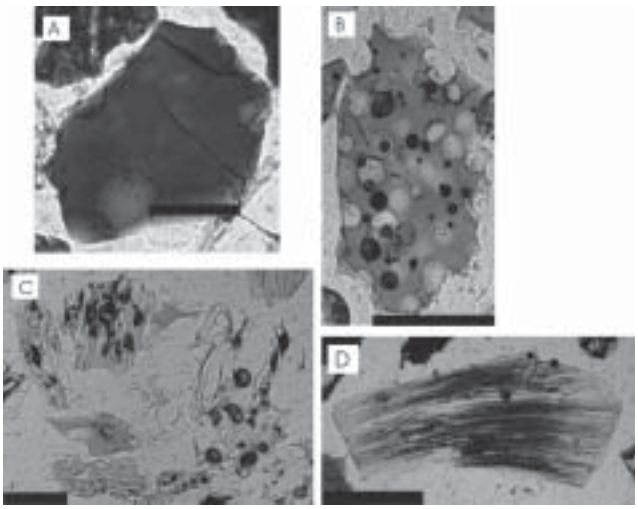

Figure 4. Transmitted light images of glass particles from the August 12-15, 1991 Hudson eruption. Note the strong contrast between different types. a) Blocky shards, dark colored and equant in shape and outlines resulting from straight to slighly irregular or concoidal fracture planes. b) Vesicular particles with low degree of vesicularity, generally equant in shape and with irregular outlines, and rounded or elongate vesicles filled by clearer fine-grained material.c) Highly vesicular particles, mostly equant in shape, with very irregular outlines and foamy texture. The outer shape of the particles is mainly the result of bubble-controlled fracturing. d) Pipe-vesicular particles are mainly whitish to light grey, show silky texture and prolated-prismatic form, sometimes twisted or bent along the «a» axis. Scale bars 100 microns long.
Figura 4. Imágenes al microscopio de polarización, sin nicoles, de las partículas vítreas de la erupción del 12-15 de Agosto de 1991 del Volcán Hudson. Nótese el fuerte contraste entre los diferentes tipo de partículas: a) Blocosas, de color oscuro y forma ecuante, con contornos resultantes de fracturas rectas, ligeramente irregulares o concoideas. b) Partículas vesiculadas con bajo grado de vesiculación, generalmente de forma ecuante y contornos irregulares, con vesículas redondeadas y alargadas rellenas por material fino de color claro. c) Partículas altamente vesiculadas, de forma mayormente ecuante, con contornos muy irregulares y estructura esponjosa. El contorno de las partículas es resultado de la fracturación de vesículas. d) Las partículas canalículo-vesiculadas son de color gris claro o blanquecino, con aspecto sedoso y forma prolada-prismática, a veces curvadas o retorcidas a lo largo del eje «a». Barra de escala de 100 micrones de largo.

we use is the fractal spectrum, a series of fractal dimensions calculated over a range of dimensional scales for each particle based on the dilation of its outline (Maria and Carey, 2002).

As there is a complete transition between non-vesicular and highly vesicular particles, the blocky and low-vesicular particles (vesicles occupy less than 20% of the clast section under the microscope) were grouped for purposes of the fractal and statistical analysis and separated from the highly-vesicular particles (vesicles occupy more than 20% of the clast section under the microscope). A few blocky particles displaying highly elongate vesicles were identified as pipe-blocky and represented separately. The different types show distinctively different behaviors on log diameter vs. fractal dimension plots. The general pattern of the fractal spectrum curves is that of increasing fractal dimension values for larger log diameter values. For some fractal spectrum curves a well-defined peak is observed at high log diameter values, followed by a regular decrease of fractal dimension values as log diameter increases (*e.g.*, Figs. 5a and 6a). To the right of these peaks the data are spurious, as a result of the complete filling of the interior of the particle outline by the dilating kernel.

Blocky particles with regular forms (B05 in Fig. 5a) have generally flat patterns with very little change in the trend of the curves. Fractal dimensions are low over a range of scales indicating an overall low degree of morphological complexity. Blocky-low-vesicular shards, such as B12 (Fig. 5a), have boundaries defined by moderate-sized vesicles and some fracture planes. Their spectra show a smooth increase in fractal

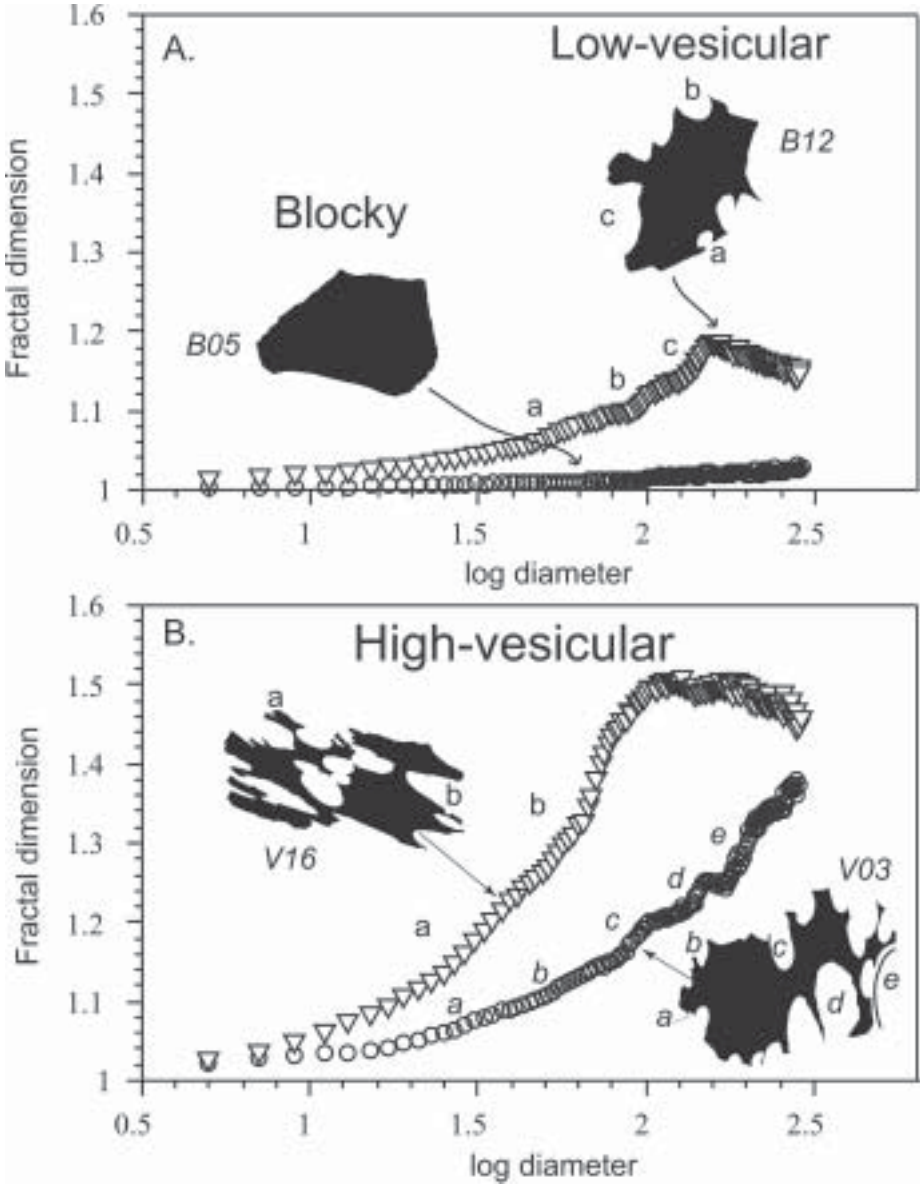

Figure 5. Fractal spectrum of selected particles. a) Blocky particle (B05) showing a flat pattern with very little change in the trend of the curve, and low fractal dimensions; low-vesicular shard (B12) with boundaries defined by moderate-sized vesicles and fracture planes and a smooth increase in fractal dimensions (a) for the smaller vesicles, followed by two increasingly steep segments (b and c) that represent larger vesicles and the wide concave fractures, respectively. b) High-vesicular particles with higher values of fractal dimensions, and curve shapes strongly controlled by the type and size distribution of vesicles. V03 boundary is defined by moderate to large oval-shaped vesicles and its fractal spectrum increases steadily but with some distinct steps (a, b, c, d, e) that relate to the increasingly larger-diameter groups of vesicles. V16 shows a steeper spectrum as result of its higher vesicularity, but lacks discrete steps because of the wider distribution of vesicle sizes. At high values of log diameter the fractal dimensions level off because of the lack of large-scale concave features.

Figura 5. Espectro fractal de partículas seleccionadas. a) Partículas blocosas (B05) con patrón plano, muy poca variación en la tendencia de la curva y baja dimensión fractal; partículas pocos vesiculadas (B12) cuyo contorno se define por vesículas de tamaño moderado y planos de fractura, con un ligero incremento en la dimensión fractal (a) para las vesículas más pequeñas seguido de dos segmentos de mayor pendiente (b, c) que representan a las vesículas mayores y a fracturas cóncavas amplias respectivamente. b) Partículas altamente vesiculadas con valores más altos de la dimensión fractal y formas curvadas fuertemente controladas por el tipo, tamaño y distribución de las vesículas. El contorno de V03 está definido por vesículas de tamaño mediano y grande y forma oval, y su espectro fractal se incrementa en forma constante pero con escalones discretos (a, b, c, d, e) que se relacionan con el incremento en el diámetro de los distintos grupos de vesículas. V16 muestra un espectro de mayor pendiente como resultado de su mayor vesiculación, pero no presenta escalones discretos porque la distribución de los tamaños de vesículas es más uniforme. Para valores más altos del logaritmo del diámetro las dimensiones fractales se nivelan por falta de rasgos cóncavos de gran escala.

dimensions (a) starting when the smaller vesicles are detected, followed by two increasingly steep segments (b and c) that represent larger vesicles and the wide concave fractures, respectively (Fig. 5a). It is inter-esting that vesicle diameters have to be concentrated around certain sizes to develop this step-like pattern. Fractal dimensions of the blocky low-vesicular particles are greater than the blocky particles reflecting the increasing complexity of the particle outlines.

As the vesicularity of the particles increases, the fractal spectra show much larger values of fractal dimensions. The shapes of the curves, however, are strongly controlled by the type and size distribution of vesicles that define the particle boundary. For example, V03 has a boundary defined by a limited number of moderate to large oval-shaped vesicles. Its fractal spectrum increases steadily, but with some distinct steps (a, b, c, d, e) that relate to the increasingly larger vesicles (Fig. 5b). The spectrum continues to rise even at high values of log diameter, reflecting the presence of large-scale concavities on the particle border. In contrast, particle V16 shows a steeper spectrum as a result of its higher vesicularity, but lacks the more discrete steps of V03 because the vesicle sizes are more evenly distributed (Fig. 5b). At high values of log diameter the fractal dimensions level off because of the lack of large scale concave features on the boundary. Pipe vesicular particles exhibit a large variety of patterns as a result of the stronger anisotrophy of particle shape (Fig. 6a). Some pipe particles (P03) show small vesicles (sections of the pipes) superimposed on an overall regular shape. Such particles often present fractures that are perpendicular to long axis of the tubular vesicles. In this case the pattern is characterized by an early rise of the fractal dimensions (a) followed by a horizontal or slightly decreasing trend (Fig. 6a). Fractal values are generally low, except for values at small length scales where the small vesicle outlines dominate the complexity of the particle boundary. A variant of this pattern is shown by particle P06, which also represents a section perpendicular to the long axis of the vesicles, but which contains the outline of larger vesicles (Fig. 6a). Its spectrum shows several distinct segments (a, b, c) that represent discontinuities in the distribution of small versus large vesicle structures on the particle boundary.

If the pipe-vesicles are larger and concentrated within a certain size, e.g. PB02 in figure 6b, a «step» pattern will arise (a), with a rapid increase in fractal dimension between two generally flat segments. Overall fractal dimension values are generally low and bear some similarity to those of blocky shards (B05, Fig. 5a). The spectrum for P11 shows a steady increase in fractal dimension with increasing log diameter, with one inflection (b) at large length scales (Fig. 6b). The steady increase is a product of the high vesicularity and wide size-range of the vesicles, and results from the intersection of micro-fractures and pipe-vesicles at relatively high angles.

The distinctive nature of the fractal spectra from different particle shapes and vesicle structures indicates that important morphological features can be captured quantitatively on a variety of spatial scales by fractal analysis. In order to test how distinct the patterns are for different particle types we have utilized multivariate statistical analysis. The results, presented in the next section, provide the basis for quantitative comparisons of the Hudson particles with those from other well-documented eruptions.

Statistical Discrimination of Different Particle Types

Principal component analysis was performed on fractal data for three sets of glass particles from: a) the August 12-15 Hudson fall deposit, b) four eruptions with inferred fragmentation mechanisms (Pacific seamount Y. Surtsey (1963). Katla (1918) and Tambora (1815), and c) groups a and b together. One hundred and forty-five variables were taken into account for each sample set, correspon ding to the complete fractal spectra of the samples. The steeply declining part of the fractal spectrum associated with spurious data was replaced by constant values in four samples of the «a» and «b» sets, respectively. The majority of the data variation can be adequately accounted for by two factors (~90% of the variation) and thus binary plots of these factors are useful for portraying morphological differences. This technique is able to effectively discriminate the four types of Hudson particles based on only two factor scores of the principal components (Fig. 7). Each particle group falls within a discrete field and there is only minor overlap. When there is overlap, as in the case of the vesicular and blocky types, it is because the transition between the two groups is actually gradational, in agreement with the observed features. It is interesting to note that even the few pipe-blocky types, showing outlines similar to the blocky group, are discriminated by the regression factor score 2, in the factor plot (Fig. 7). Low values of factor score

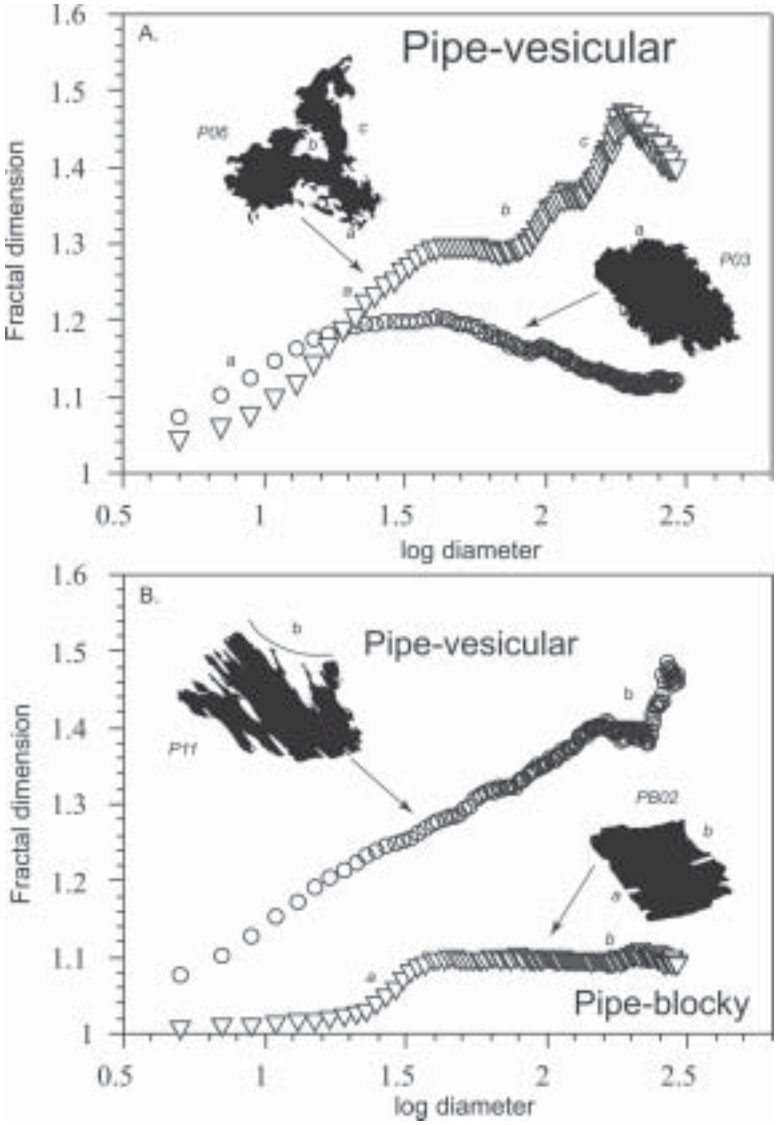

Figure 6. Fractal spectrum of selected particles. a) Sections oblique or perpendicular to the long axis of the vesicles in pipe vesicular particles (P03) contain fine-scale complexity superimposed on an overall regular shape. The pattern is characterized by an early rise of the fractal dimensions (a) followed by a horizontal or slightly decreasing trend. Fractal values are low, except for values at small length scales where the small vesicle outlines dominate the complexity of the particle boundary. P06 spectrum shows several distinct segments (a, b, c) that represent discontinuities between the distribution of small versus large coalescent vesicle structures on the particle boundary. b) «Step» pattern arising from a single population of vesicles intersected at low angle (a in PB02), showing a rapid increase in fractal dimension between two generally flat segments. In P11 the long axis of the clast is parallel to the pipe vesicles and the spectrum shows a steady increase in fractal dimension with an inflection (b) at large length scale. The steady increase is a product of the large vesicularity and wide size-range of vesicles, that result from the vesicle coalescence and from the intersection of microfractures and pipe-vesicles.

Figura 6. Espectro fractal de partículas seleccionadas. a) Secciones oblicuas o perpendiculares al eje mayor de las vesículas en vesículas canalículo-vesiculadas (P03) que generan complejidad de pequeña escala sobreimpuesta a una forma general simple. El patrón se caracteriza por un aumento inicial de la dimensión fractal (a) seguido por una tendencia horizontal o ligeramente decreciente. Los valores fractales son bajos, con la excepción de los que corresponden a longitudes pequeñas en las cuales las vesículas de tamaño pequeño producen formas complejas en el borde de la partícula. El espectro de P06 evidencia varios segmentos (a, b, c) que representan discontinuidades entre la distribución de vesículas pequeñas vs grandes estructuras vesiculares formadas por la coalescencia de vesículas menores. b) Patrón escalonado que surge de poblaciones simples de vesículas-canalículo seccionadas paralelamente al eje mayor («a» en PB02), y que muestran un rápido incremento en la dimensión fractal entre dos segmentos generalmente planos. En P11 el eje mayor del clasto es paralelo a los canalículos y el especto muestra un incremento constante en la dimensión fractal con una inflexión (b) en las longitudes mayores. El incremento constante es producto de la gran vesiculación y del gran rango de tamaño de las vesículas que resulta de la coalescencia de vesículas menores, y de la intersección de microfracturas y canalículos.

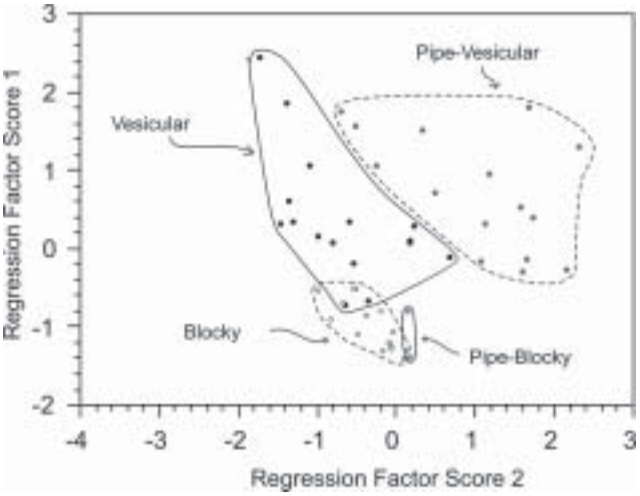

Figure 7. Binary plot of factor scores 1 and 2 from principal component analysis of fractal spectrum data for the four primary types of glassy ash particles from the August 12-15 Hudson eruption. Note the good separation of particle types based on the fractal analysis of the particle outlines.

Figura 7. Gráfico binario de los «scores» de factores 1 and 2 procedentes del análisis de componentes principales de los datos del espectro fractal para los cuatro tipos principales de partículas vítreas de la erupción del 12 al 15 de agosto del Volcán Hudson. Nótese la buena separación entre los distintos tipos de partículas basado en el análisis fractal de los contornos.

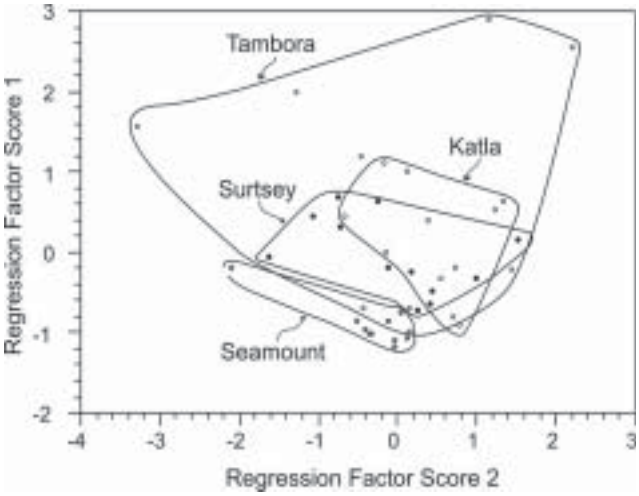

Figure 8. Binary plot of factor scores 1 and 2 from principal component analysis of fractal spectrum data for glassy ash particles from a Pacific seamount, the 1963 eruption of Surtsey in Iceland, the 1918 eruption of Katla volcano in Iceland and the 1815 eruption of Tambora in Indonesia.

Figura 8. Gráfico binario de los «scores» de factores 1 and 2 procedentes del análisis de componentes principales del espectro fractal de partículas vítreas de ceniza de una montaña submarina del océano Pacífico, de la erupción de 1963 del Volcán Surtsey en Islandia, de la erupción de 1918 del Volcán Katla en Islandia y de la erupción de 1815 del Volcán Tambora en Indonesia.

1 typically correspond to simple particle boundaries with little small-scale complexity (Maria, 2000). Increasing values of factor score 1 are reflected in increasing degrees of complexity as defined by the intersection of remnant vesicles and the particle boundary. Low values of factor score 2 also correspond to relatively simple particle boundaries, whereas higher values are typically associated with more complex boundaries defined by larger remnant vesicles (Maria, 2000).

Fractal analysis was also carried out on a series of samples from eruptions with different fragmentation mechanisms in order to make comparisons with the Hudson tephra. A sample collected from Pacific seamount Y at >2000 m depth consists of basaltic glasses that formed by quench granulation fragmentation associated with the non-explosive interaction of magma and seawater (Batiza *et al.*, 1983). The particles are devoid of vesicles and exhibit simple conchoidal-shaped boundaries. A sample from the 1963 eruption of Surtsey volcano in Iceland consists of moderately vesicular scoria that was produced by phreatomagmatic eruptions as the island grew from a shallow subaqueous vent to a subaerial edifice (Moore, 1985). A sample of 1918 tephra fall from Katla volcano in Iceland consists of well-vesicular scoria that was produced by phreatomagmatic eruptions from a subglacial source vent (Larsen, 2000). The high degree of vesicularity of the Katla sample relative to the Surtsey sample indicates that exsolution of primary volatiles was also an important driving force of the eruption. Finally, a sample from the 1815 tephra fall of Tambora volcano in Indonesia consists of a mixture of moderate to highly vesicular trachyandesite micropumice and less abundant blocky shards. The primary mechanism of fragmentation during the Tambora eruption is thought to be degassing of primary volatiles with H_2O as high as 5.0% (Sigurdsson and Carey, 1989). The Tambora sample is particularly useful as the magma composition is close to that of the Hudson magma. These samples thus represent a range of fragmentation mechanisms from purely external magma/water interactions (non-explosive) to explosive disruption driven dominantly by exsolution of primary volatiles.

Principal component analysis of the seamount, Surtsey, Katla, and Tambora samples results in the creation of different fields for each fragmentation mechanism on a plot of the two major factor scores

(Fig. 8). Particles produced solely by magma/water interactions (Pacific seamount) form a relatively tight grouping with low values of factor scores 1 and 2. The Surtsey particles extend towards slightly more complex shapes than the Pacific seamount ones. The Katla samples overlap with the Surtsey samples and extend to more complex shapes with relatively high values of factor score 1. This is in accord with the observation that the Katla samples are more highly vesicular than the Surtsey samples and likely involved more extensive degassing of dissolved volatile components. The most diverse and extensive field is defined by the Tambora samples (Fig. 8). It extends to the highest values of both factor scores but also overlaps partially with the simple boundaries of the seamount, and completely with the Surtsey and Katla samples. The Tambora particles thus exhibit the greatest overall diversity in boundary complexity. However, a significant proportion of the Tambora particles are characterized by highly complex shapes, reflecting their high degree of vesicularity. Only a few of the Tambora particles exhibit shapes that are more blocky in character. Even these particles show many small vesicles and similar color to the vesicular particles. The same is not true for the Hudson blocky particles which are darker than the vesicular ones, and sometimes completely devoid of vesicles.

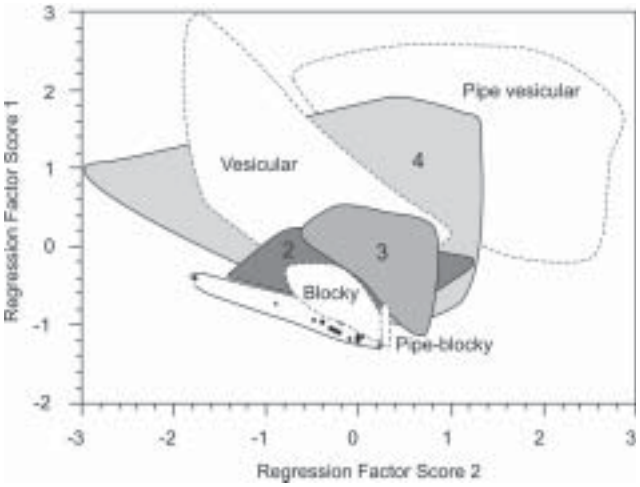

Figure 9. Comparison of Hudson tephra particles with particles from eruptions of known fragmentation mechanism based on factor analysis of fractal spectrum data. 1. Pacific seamount, 2. Surtsey (1963), 3. Katla (1918), 4. Tambora (1815).

Figura 9. Comparación de las partículas de tefra del Hudson con partículas de erupciones cuyos mecanismos de fragmentación son conocidos, basada en datos del análisis de factores. 1. Montaña submarina del Océano Pacífico, 2. Volcán Surtsey (1963), 3. Volcán Katla (1918), 4. Volcán Tambora (1815).

A statistical comparison of the Hudson tephra with the other particles from eruptions of known fragmentation style illustrates the great diversity of the Hudson tephra (Fig. 9). Blocky and pipe blocky shards from the eruption show strong similarities to particles formed during purely magma/water interactions and phreatomagmatic explosions in shallow subaqueous conditions. Vesicular particles are similar to the field of 1815 Tambora particles formed primarily by degassing of volatile-rich trachyandesite magma and the Katla particles produced by phreatomagmatic eruptions of a basaltic magma with enough dissolved volatiles to produce extensive vesiculation (Fig. 9). The pipe vesicular particles of the Hudson eruption also overlap with the Tambora field, but extend to higher degrees of boundary complexity.

SEM Imaging of Glassy Particles

We attempted to identify additional evidence for the magma/water interactions by using SEM imaging of the Hudson particles. Recent work by Buttner et al (1999) has shown that a characteristic feature of magma-water interactions that involve relatively large amounts of external water is the formation of hydration cracks on the surface of glassy particles. Such cracks are interpreted to have formed on the glassy surfaces of particles shortly after fragmentation as the particles interact with excess external water that has not been converted to superheated steam. Figure 10 illustrates the diversity of particle vesicularity types amongst the glassy tephra particles. A search of more than 100 mounted particles revealed no evidence of hydration cracks on the particle surfaces. Instead, glassy particles had surfaces that were generally smooth (Fig. 11a) or with slight evidence of step-like features (Fig. 11b).

The lack of hydration cracks, but the presence of abundant blocky type particles with step-like features, suggests that the fragmentation mechanism for some of the particles falls into the category of «dry» magma-water interactions based on the model of Buttner *et al.* (1999).

CHEMICAL COMPOSITION OF GLASSY HUDSON TEPHRA

Previous analyses of samples from Hudson Volcano range from basalt to dacite, suggesting a bimodal calc-

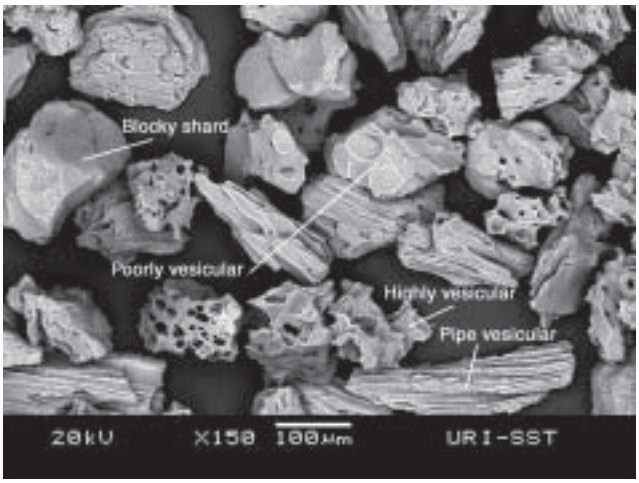

Figure 10. SEM photograph of glassy tephra particles from the August 12-15, 1991 Hudson eruption. Note the large variation in degrees of vesicularity exhibit by the particles. Scale bar is 100 microns in length.
Figura 10. Fotografías de Microscopio Electrónico de Barrido de partículas vítreas de ceniza de la erupción del 12-15 de agosto de 1991 del Volcán Hudson. Nótese la gran variación en el grado de vesiculación que muestran la partículas. La barra de escala tiene 100 micrones de largo.

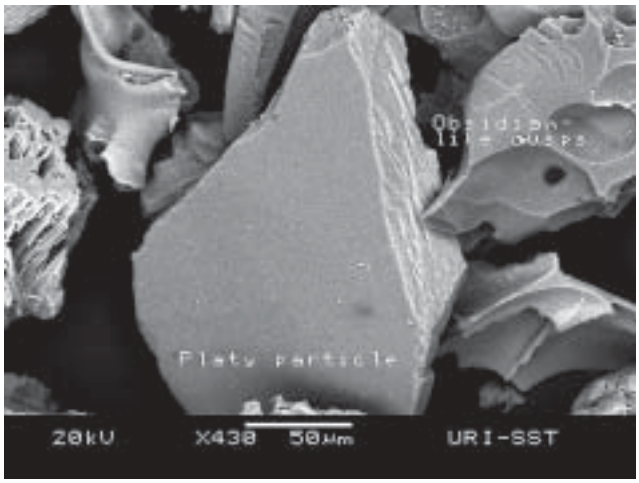

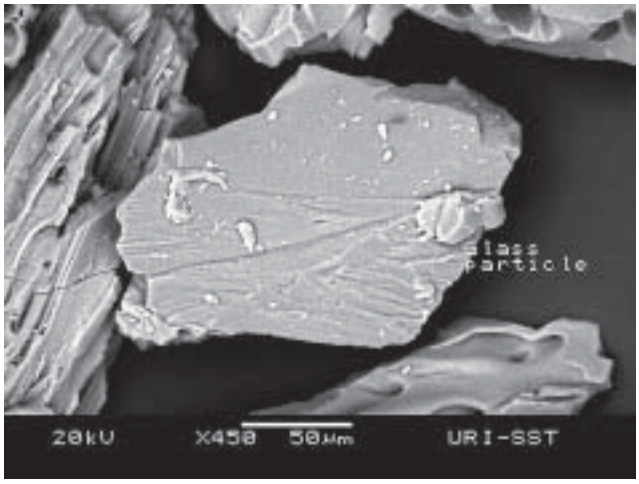

Figure 11. SEM photographs of glassy tephra particles from the August 12-15, 1991 Hudson eruption showing a) a smooth surface on a blocky particle and b) a stepped surface on a blocky particle. Scale bars are 50 microns in length.
Figura 11. Fotografías de Microscopio Electrónico de Barrido de partículas vítreas de tefra de la erupción del 12-15 de agosto de 1991 del Volcán Hudson a) una superficie lisa en una partícula blocosa algo aplanada b) una superficie escalonada en una partícula blocosa. Barras de escala de 50 micrones de largo.

alkaline suite. Their characteristics are medium- to high-K_2O content, with relative enrichment of TiO_2 , Na_2O, and incompatible trace elements (including large-ion-lithophile, rare-earth, and high-field-strength elements) compared with samples of similar silica content from other volcanoes in the southern Andean volcanic zone (Stern, 1991; Naranjo and Stern, 1998; see also Fuenzalida, 1976; Godoy *et al.,* 1981; Notsu *et al.,* 1987; Futa and Stern, 1988; Naranjo *et al.,* 1993; Bitschene and Fernández, 1995). No major or progressive changes in magma composition during the August 12-15, 1991 eruption were detected in the distal fall deposits.

Analyses of silicic glasses from the August 12-15 fall deposit by Bitschene and Fernández (1995) exhibit a bimodal distribution with a dominant dacitic composition, encompassing a SiO_2 range of only a few percent, and a subordinate population of rhyodacitic composition. Analyses performed on dark glass show only a small decrease in silica and slight increase in MgO, TiO_2 and CaO relative to the colorless glass (Nillni *et al.,* 1992; Bitschene and Fernández, 1995). We have analyzed glassy shards representing the four major morphological types and there is no evidence of mixed magmas on the scale of individual shards, even though some particles display distinct banding in color (Fig. 12). The glasses exhibit a small range in composition with silica content between 61.5 and 65.0 wt.%, but with the majority falling in a narrow group between 63-64% SiO2. We did not find any systematic correlation between morphological type and composition, as suggested by Bitschene and Fernandez (1995). Thus, the morphological and color differences do not appear to be strongly related to magma composition.

DISCUSSION

Glassy dacitic tephra from the August 12-15, 1991

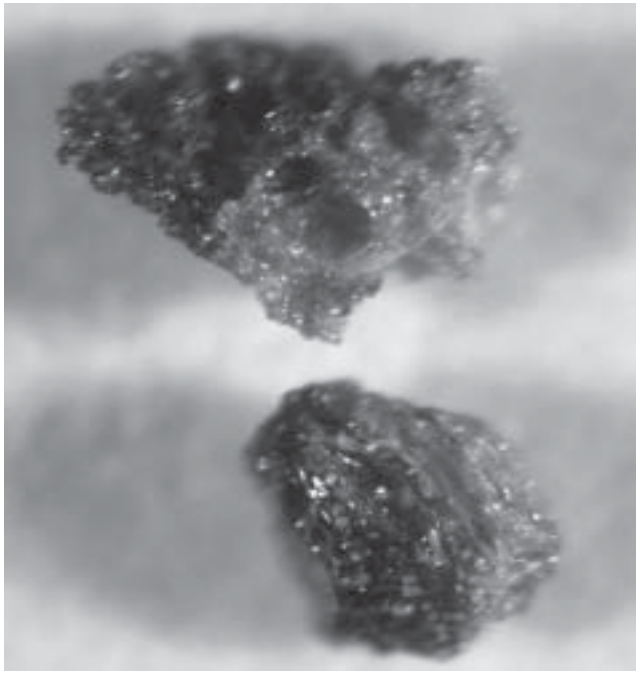

Figure 12. Glassy ash particle from the August 12-15 Hudson eruption showing different glass colors in a single particle. Particles are approximately 1 mm in length.
Figura 12. Partículas vítreas de ceniza de la erupción del 12-15 de agosto del Volcán Hudson, que muestran diferentes colores en el vidrio dentro de la misma partícula. Las partículas son de aproximadamente 1mm de largo.

Hudson tephra fall displays a remarkably wide variety of particle morphologies and color. Vesicularity, color and external form were the main attributes used to group particles into several types of categories. Vesicularity is largely an internal feature that is likely to contribute to a particle's characteristic outline after fragmentation. Thus, the outline of every particle has a definite fractal spectrum which is mainly a function of the extent, size and type of vesicles present at the moment of fragmentation. Discrete steps with steeper slopes in the fractal spectrum reflect more abundant vesicles grouped around certain sizes. Fractal analysis of only the particle boundaries coupled with factor analysis of the resulting fractal spectra is able to distinguish particles that were grouped largely by their degree and nature of internal vesiculation (Fig. 7). Bubble size and population are in turn related to bubble nucleation and coalescence in the magma before or during fragmentation (Klug *et al.,* 2002). Thus, the extent and structure of vesiculation clearly impart a characteristic control on the final morphology of a particle's external boundary and allows quantitative discrimination of particle types by fractal analysis. Fragmentation of viscous, vesiculating magma is a complex and still incompletely understood process (Alidibirov and Dingwell, 1996, 2000; Sahagian, 1999; Klug *et al.,* 2002). As bubbles grow the interstitial magma viscosity increases dramatically due to the loss of volatile components by diffusion and stresses buildup during magma ascent. One model suggests that fragmentation occurs when the tensile stress at the inner walls of bubbles exceeds the tensile strength of the magma (Zhang, 1999). Alternatively, increasing strain rates during magma ascent in a conduit results in crossing of the glass transition point with subsequent brittle failure of bubble-rich magma (Papale, 1999). In addition, interaction with external water and subsequent explosions and/or chilling is an efficient mechanism to fragment magma (Wohletz, 1983, 1986; Zimanowski *et al.,* 1997). Previous studies have suggested that the relative roles of primary volatile degassing versus hydromagmatic activity during explosive eruptions can be assessed by examining the morphology of the resulting particles (e.g. Sheridan and Marshall, 1983; Sheridan and Wohletz, 1983). Primary volatile degassing produces highly vesicular particles whose external boundaries are strongly controlled by the size, number, and shape of vesicles in the magma just prior to fragmentation. Hydromagmatic fragmentation typically produces particles that have a more blocky morphology and whose external boundary is controlled by a combination of brittle fractures and, to a lesser extent, the shapes of pre-existing vesicles. However, most assessments of fragmentation mechanisms have relied largely on qualitative comparisons of particle morphologies.

Fractal analysis of the 1991 Hudson tephra and particles from other eruptions of inferred fragmentation styles allows for quantitative comparisons of particle morphologies in order to assess processes during the paroxysmal phase of the Hudson event. Blocky and low vesicularity particles from the Hudson eruption show similar fractal characteristics to particles produced by quench fragmentation (seamount samples) and phreatomagmatic eruptions (Katla tephra, Fig. 9). The abundance of these particles in the Hudson fall deposit indicates that external water played a significant role in the fragmentation of the trachyandesite magma erupted on August 12-15, 1991, as was previously suggested (Destéfano and Mazzoni, 1992; Mazzoni and Destéfano, 1992). SEM imaging of particles suggests that the magma-water was of the «dry» variety with lack of excess external water in liquid form

(Büttner *et al.,* 1999).

In addition, however, a large number of the particles exhibit morphological characteristics similar to those fragments produced by degassing of dissolved volatile components, such as those from the 1815 eruption of Tambora volcano in Indonesia (Fig. 9). Vesiculation and fragmentation by downward passage of a release wave generating tensile stresses in acidic magmas are regarded as the major causes of particle formation in explosive eruptions (Alidibirov and Dingwell, 1996, 2000; Klug *et al.,* 2002). When tensile stresses exceed the dynamic tensile strength of the already vesiculated magma fragmentation and fracturing occur and the resulting fragments may show outlines with different orders of irregularities. Two irregularity scales were described in a fractal analysis of magmatic particle boundaries from the Monte Pilato-Rocche Rosse eruptions, carried out by Dellino and Liotino (2002). These irregularities correspond to textural and structural fractal elements. The latter reflects the larger boundary irregularities, related to vesicles. The textural fractal is not related to vesicles but to brittle fracturing of the melt (Dellino and Liotino, 2002) as it was previously suggested by Carey *et al.* (2000) for phreatomagmatic fragmentation. Hudson pumice and shard outlines show a widely variable contribution of both vesicle and fracture planes. Vesicle-shaped boundaries are almost lacking in the blocky particles, but they make up most of the boundaries in the highly-vesicular particles. The fractal spectra not only record the fracture and vesicle contributions but also the different modes in vesicle size. Thus, it results a useful tool for characterization of the particles and their origin.

We suggest that the diversity of particle morphologies found in the August 12-15, 1991 Hudson tephra fall was the result of a combination of fragmentation by degassing of primary volatile components and transient interactions with external water. A relatively large volume (> 4 km^3) of homogenous trachyandesite magma existed in a crustal reservoir prior to the 1991 eruptions (Fig. 13). This magma probably contained several wt.% H2O dissolved in the dacitic melt phase, although it may not have been volatile-saturated as amphibole was not present amongst the crystal assemblage (Bitschene and Fernandez, 1995). During the initial basaltic phase of the eruption and at the onset of the August 12-15 paroxsymal phase, extensive subglacial melting of the ice-filled summit caldera occurred. This provided an important source of external water for interaction with

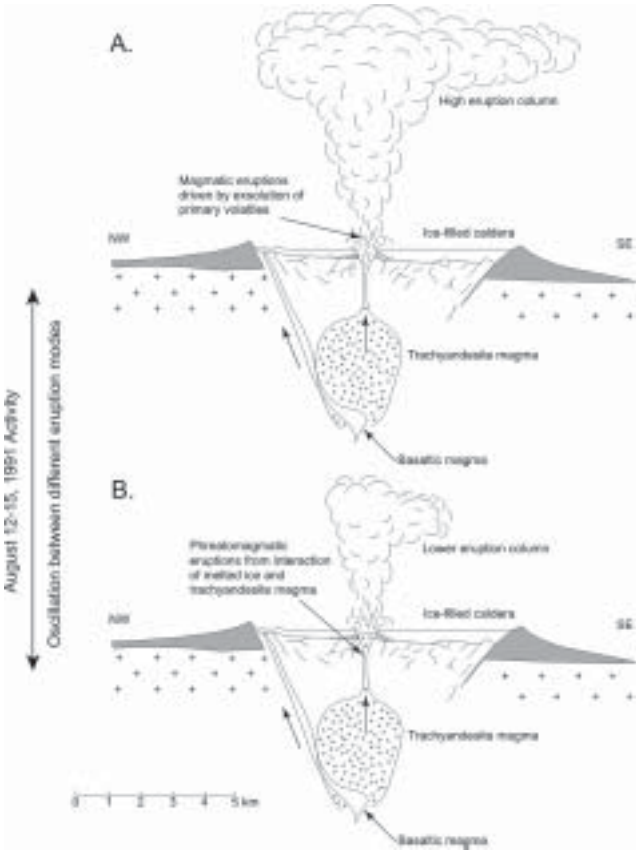

Figure 13. Suggested eruption modes during the August 12-15, 1991 climactic eruption of Hudson volcano. a). Explosive eruption of trachyandesite magma driven principally by exsolution of dissolved volatile generates high eruption column and vesicular glassy tephra. b) Interaction of meltwater from the ice-filled caldera and trachyandesite magma results in phreatomagmatic explosions that generate relatively low eruption columns and poorly-vesicular glassy tephra. Some of the interactions are likely to have occurred at depth within the conduit where the local pressure was sufficiently high to inhibit vesiculation from primary dissolved volatiles. Observed variations in eruption column height and nature of glassy particles generated during the August 12-15 period suggest oscillation between these two types of eruption mechanisms.

Figura 13. Estilos eruptivos que se proponen para la erupción del 12-15 de agosto de 1991 del volcán Hudson. a) Erupción explosiva de magma traquiandesítico, principalmente impulsada por la exolución de volátiles, que genera una elevada columna eruptiva y tefras vítreas vesiculadas. b) Interacción entre aguas de fusión del relleno de hielo de la caldera y el magma traquiandesítico, que produce erupciones freatomag-máticas con columnas eruptivas más bajas y tefras poco vesiculadas. Algunos de estos últimos episodios pro-bablemente ocurrieron en profundidad dentro del conducto, en donde la presión local fue suficientemente alta como para inhibir la vesiculación. Las variaciones que se observan en la altura de la columna eruptiva y en la naturaleza de las partículas vítreas que se generaron durante la erupción del periodo del 12 al 15 de agosto sugieren una oscilación entre ambos tipos de mecanismos eruptivos.

magma. The stratigraphy of the August 12-15 fall deposit (Scasso *et al.,* 1994) and observations of eruption column height variations (Naranjo *et al.,* 1993) indicate that the paroxsymal phase of the eruption consisted of a series of at least three major pulses of explosive volcanism. The pulsatory nature of this phase of the eruption may have resulted from discrete discharges of trachyandesite magma that fragmented by primary volatile degassing, but with the pulses initiated and/or modulated by phreatomagmatic events when magma interacted with melt water. Rapid pressure reduction caused by phreatomagmatic vent clearing may have induced further vesiculation and fragmentation by downward passage of a release wave generating tensile stresses in the magma (Heiken and Wohletz, 1991; Alidibirov and Dingwell ,1996, 2000; Klug *et al.,* 2002).

A series of these eruptive cycles could explain the diversity of particle types found in the fall deposits and the observed pulsatory nature of the August 12-15 activity. The cyclic nature of the activity may be related to the time necessary to build-up subglacial reservoirs of melt water between eruptive pulses and the ability of the crustal reservoir to supply viscous trachyandesitic magma to the surface.

The August 12-15 eruptive phase did not appear to discharge any of the basaltic magma that was involved in the initial August 8 eruption. Naranjo *et al.* (1993) proposed that the basaltic magma bypassed the chamber containing the trachyandesite magma and erupted in an area peripheral to the vent of the paroxsymal eruption. Despite the lack of basaltic glasses in the August 12-15 eruption, the influx of mafic magma from depth may have played an important role in the overall eruption. Triggering of explosive eruption by influx of mafic magma at the base of a crustal reservoir has been proposed for many siliceous events (e.g. Sparks *et al.,* 1977; Pallister *et al.*, 1992). If an influx of mafic magma did trigger the eruption, then the lack of evidence for magma mixing in the August 12-15 Hudson tephra indicates that the basaltic magma was unable to penetrate and intermingle with the dominant trachyandesite magma. This may have been the result of a large density contrast between the basalt with the trachyandesite leading to a stable pooling of the basalt at the base of the magmatic system. Eruption of the basalt at vents along the caldera rim at the onset of eruptive activity may have been facilitated by faults that provided a pathway for magma to reach the surface. However, the influx of basaltic magma at the base of the trachyandesite reservoir may have led to heating of the magma and subsequent supersaturation of volatiles (Blake, 1984). The presence of resorbed phenocrysts and small scale variations in glass chemistry may be the best evidence for basalt influx beneath the trachyandesite.

CONCLUSIONS

Glassy tephra from the August 12-15, 1991 plinian eruption of Hudson volcano in Chile show a wide variety of particle shapes and color, ranging from dark, poorly-vesicular shards to light-colored, pipe-vesicular micropumice. The outlines of different particle types have a characteristic fractal spectrum that is mainly a function of the extent, size, and type of vesicles present at the moment of fragmentation. Discrete steps within the fractal spectra reflect an abundance of vesicles centered around particular sizes.

Glassy particles originally grouped by their internal vesicle populations are well discriminated by principal component analysis of the fractal spectrum of their outlines into four principal types: blocky, vesicular with spherical vesicles, pipe vesicular and pipe-blocky. Thus, the analysis of the particle outlines provide a powerful tool to define the type and extent of internal vesicularity.

A quantitative comparison of particle shapes using factor analysis of fractal spectrums of the 1991 Hudson tephra with other tephra produced by eruptions with well constrained fragmentation styles indicates that production of the Hudson tephra involved both interaction of magma with external water and exsolution of dissolved volatiles. SEM imaging of particles suggests that the magma-water was of the «dry» variety with lack of excess external water in liquid form.

Extensive subglacial melting of the ice-filled summit caldera provided an important source of external water for interaction with magma. The pulsatory nature of the paroxsymal phase of the eruption may have resulted from discrete discharges of trachyandesite magma that fragmented by primary volatile degassing but which were initiated by phreatomagmatic events. Transient clearing of the vent and conduit may have led to fragmentation of volatile-rich trachyandesitic magma, *via* volatile exsolution due to rapid ascent (or downward pressure release), producing highly vesicular particles.

In contrast to the initial, August 8 eruption, the August 12-15 eruptive phase did not discharge significant amounts of basaltic magma. However, the influx of mafic magma from depth may have played an

important role, triggering the explosive eruption by heating the trachyandesitic magma and promoting volatile supersaturation, as is suggested by the presence of resorbed phenocrysts and small-scale variations in glass chemistry.

Acknowledgements: R.A.S. wishes to acknowledge the United States Fulbright Program for providing a grant for travel to the University of Rhode Island in the fall of 2002. Joe Devine provided invaluable assistance and expertise during microprobe analysis of glass particles at Brown University. Useful comments by the reviewers, R. Cas and J. White, helped to improve the manuscript.

References

Alidibirov, M. and D. Dingwell, 1996. Magma fragmentation by rapid decompression. *Nature* 380:146-148.

Alidibirov, M. and D. Dingwell, 2000. Three fragmentation mechanisms for highly viscous magma under rapid decompression. *Journal of Volcanological and Geothermal Research* 100:413-421.

Arias, N., A. Arizmendi, P. Bitschene, M. Fernández, R. Giacosa, M. Griznik, M. Márquez and A. Nillni, 1992. La erupción del volcán Hudson y sus efectos inmediatos en la Patagonia argentina (Provincia de Santa Cruz). *Primera Reunión Argentina de Mineralogía y Metalogenia*, Actas: 9-18.

Banks, N.G. and M. Iven, 1991. *Report of the United Nations Mission to Volcán Hudson, Chile, 20 August - 15 September 1991*. Unpublished Report, US Geological Survery, Cascades Volcano Observatory, pp 1-61.

Batiza, R., D. Fornari, D. Vanko and P. Lonsdale, 1984. Craters, calderas, hyaloclastites on young Pacific Seamounts. *Journal of Geophysical Research* 89: 8371-8390.

Best, J.L., 1992. Sedimentology and event timing of a catastrophic volcaniclastic mass flow, Volcaán Hudson, southern Chile. *Bulletin of Volcanology* 54:299-318.

Bitschene, P. and M.I. Fernández, 1995. Volcanology and petrology of fallout ashes from the August 1991 eruption of the Hudson volcano (Patagonian Andes). En: J. Mendía y P. Bitschene (eds), *The August 1991 eruption of the Hudson volcano (Patagonian Andes): a thousand days after*. Publicación Especial de la Universidad Nacional de la Patagonia San Juan Bosco y Servicio Nacional de Geología, pp.27-54, Comodoro Rivadavia, Argentina.

Bitschene, P., M. Fernández, N. Arias, A. Arizmendi, M. Grizinik and A. Nillni, 1993. Volcanology and environmental impact of the August 1991 eruption of the Hudson volcano (Patagonian Andes, Chile). *Zentralbaltt für Geologie und Palaeontologie*, Teil 1/2: 165-177.

Blake, S., 1984. Volatile Oversaturation During the Evolution of Silicic Magma Chambers as an Eruption Trigger. *Journal of Geophysical Research* 89:8237-8244.

Buttner, R., P. Dellino and B. Zimanowski, 1999. Identifying magma-water interaction from the surface features of ash particles. *Nature* 401:688-690.

Carey, S. and H. Sigurdsson, 1982. Influence of particle aggregation on deposition of distal tephra from May 18, 1980 eruption of Mount St. Helens volcano. *Journal of Geophysical Research* 87:7061-7072.

Carey S, Sigurdsson H, Gardner JE, Criswell W, (1990) Variations in column height and magma discharge during the May 18, 1980 eruption of Mount St. Helens. Journal of Volcanological and Geothermal Research, 43:99-112

Carey, S., Maria, A. and H. Sigurdsson, 2000. Use of fractal analysis for discrimination of particles from primary and reworked jökulhlaup deposits in SE Iceland. *Journal of Volcanology and Geothermal Research* 104:65-80.

Carey, S., D. Morelli and H. Sigurdsson, 2001. Tsunami deposits from major explosive eruptions: an example from the 1883 eruption of Krakatau. *Geology* 29: 347-350.

Corbella, H., R.A. Scasso, M. Lucero, M.E. Palacios, P.E. Tiberi, P. Rial and D. Pérez, 1991a. Erupción del Volcán Hudson - Agosto de 1991. Efectos sobre el territorio de la Provincia de Santa Cruz. *Publicación Científica de la Universidad Federal de la Patagonia Austral, Waxen* 4:1-15.

Corbella, H., R.A. Scasso, P. Rial, M.E. Palacios, M. Lucero, P.E. Tiberi and D. Pérez, 1991b. Hudson. *Bulletin of the Global Volcanism Network* 16:2-3.

Criswell, W., 1987. Chronology and pyroclastic stratigraphy of the May 18, 1980 eruption of Mount St. Helens. *Journal of Geophysical Research* 92: 10237-10266.

Dellino, P. and L. LaVolpe, 1996. Image processing analysis in reconstructing fragmentation and transportation mechanisms of pyroclastic deposits.

The case of Monte Pilato-Rocche Rosse eruptions, Lipari (Aeolian Islands, Italy). *Journal of Volcanological and Geothermal Research* 71:13-19.

Dellino, P. and G. Liotino, 2002. The fractal and multifractal dimension of volcanic ash particles contour: a test study on the utility and volcanological relevance. *Journal of Volcanological and Geothermal Research* 113: 1-18 .

Destéfano, M.C. and M.M. Mazzoni, 1992. Textura superficial y composición de trizas vítreas de la erupción 1991 del volcán Hudson. *Cuarta Reunión Argentina de Sedimentología,* Actas 1:211-218. La Plata.

Flook, A.G., 1978. The use of dilation logic on the Quantimet to achieve fractal dimension characterization of textured and structural profiles. *Powder Technology* 21:295-298.

Fuenzalida, R., 1976. The Hudson volcano. *IAVCEI Symposium on the Andean and Antarctic Volcanology problems*, Proceedings 143-171.

Fuenzalida, R. and W. Espinosa, 1974. Hallazgo de una caldera volcánica en la provincia de Aisén. *Revista Geológica de Chile* 1:64-66.

Futa, K. and C. R. Stern, 1988. Sr and Nd isotopic and trace element compositions of Quaternary volcanic centers of the southern Andes. *Earth and Planetary Science Letters* 88:253-262.

Godoy, E., M. Dobbs and C.R. Stern, 1981. El volcán Hudson, primeros datos geoquímicos e isotópicos en coladas interglaciares. *Comunicaciones* 32:1-9. Comunicaciones Departamento de Geología, Facultad de Ciencias Físicas y Matemáticas de la Universidad de Chile, Santiago de Chile.

Heiken, G. and K. Wohletz, 1985. *Volcanic ash*. University of California Press, Berkeley, 246 pp.

Heiken, G. and K. Wohletz, 1991. Fragmentation processes in explosive volcanic eruptions. En R.V. Fisher y G.A. Smith (eds), *Sedimentation in Volcanic Settings*, Society of Economic Paleontologists and Mineralogists, Special Publication 45:19-26.

Hildreth, W. and R.E. Drake, 1992. Volcán Quizapu, Chilean Andes. *Bulletin of Volcanology* 54:93-125.

Klug, C., K.V. Cashman and C.R. Bacon, 2002. Structure and physical characteristics of pumice from the climactic eruption of the Mount Mazama (Crater Lake), Oregon. *Bulletin of Volcanology* 64:486-501.

Larsen, G., 2000. Holocene eruptions within the Katla volcanic system, south Iceland: characteristics and environmental impact. *Jokull* 49:1-28

Maria, A., 2000. *Volcanic particles and fractal analysis*. PhD. Thesis, Graduate School of Oceanography, University of Rhode Island, 197 pp.

Maria, A. and S. Carey, 2002. Using fractal analysis to quantitatively characterize the shapes of volcanic particles. *Journal of Geophysical Research* 107(B11), 2283, doi:10.1029.2001Jb000822, 2002.

Mazzoni, M.M. and M.C. Destéfano, 1992. Depositación sineruptiva y reelaboración temprana. Depósitos de caída de ceniza de la erupción 1991 del volcán Hudson. *Cuarta Reunión Argentina de Sedimentología,* Actas 1:203-210. La Plata.

Moore, J.G., 1985. Structure and eruptive mechanism at Surtsey volcano, Iceland. *Geological Magazine* 122: 649-661.

Morelli, D., 2002. *Fractal analysis of pumice, Krakatau, 1883*. Masters thesis. Graduate School of Oceanography, University of Rhode Island, 74 pp.

Naranjo, J., 1991 Major eruption reported in Chile. *EOS Transactions of the American Geophysical Union* 72:393-394.

Naranjo, J.A, H. Moreno and N.G. Banks, 1993. La erupción del volcán Hudson en 1991 (46°S), Región XI, Aisén, Chile. *Servicio Nacional de Geología y Minería – Chile, Boletín* 44:1-50.

Naranjo, J.A. and C.R. Stern, 1998. Holocene explosive activity of Hudson Volcano, southern Andes. *Bulletin of Volcanology* 59:291-306.

Nillni, A. and P. Bitschene, 1995. Sedimentología y procesos de depositación de la tefra de caída de la erupción del volcán Hudson en agosto 1991. En J. Mendía y P. Bitschene (eds), *The August 1991 eruption of the Hudson volcano (Patagonian Andes): a thousand days after*. Publicación Especial, Universidad Nacional de la Patagonia San Juan Bosco y Servicio Nacional de Geología, 116-134, Comodoro Rivadavia, Argentina.

Nillni, A., M. Fernández, A. Arizmendi, N. Arias, M. Rodríguez and P. Bitschene, 1992. Volcán Hudson: estudio granulométrico y composicional del material piroclástico eyectado. *Cuarta Reunión Argentina de Sedimentología,* Actas 3:73-80. La Plata.

Notsu, K., L. López and N. Onuma, 1987. Along-arc variations in Sr-isotopic compositions in volcanic rocks from the southern Andes (33S-55S). *Geochemical Journal* 21: 07-313.

Orihashi, Y., J.A. Naranjo, A. Motoki, H. Sumino, D. Hirat, R. Anma and K. Nagao, 2004. Quaternary volcanic activity of Hudson and Lautaro volcanoes, Chilean Patagonia: New constraints from K-Ar ages. *Revista Geológica de Chile* 31:207-224

Pallister, J., R. Hoblitt and A. Reyes, 1992. A basalt trigger for the 1991 eruptions of Pinatubo volcano? *Nature* 356:426-428.

Papale, P., 1999. Strain-induced magma fragmentation in explosive eruptions. *Nature* 397:425-428.

Richardson, L.F., 1961. The problem of contiguity. En A. Rapaport, L. von Bertalanfy y R. Meier (eds), *General System*. Yearbook for the Society for General Systems Research, 6 pp. 139-187.

Sahagian, D., 1999. Magma fragmentation in eruptions. *Nature* 402:589-591.

Sarna-Wojicki AM, Shipley S, Waitt R Jr, Dzurisin D, Wood S (1982) Areal distribution, thickness, mass, volume and grain-size of air-fall ash from six major eruptions of 1980. US Geological Survey, Professional Paper 1250:577-600

Scasso, R.A., H. Corbella and P. Tiberi, 1994. Sedimentological analysis of the tephra from the 12-15 August 1991 eruption of Hudson volcano. *Bulletin of Volcanology* 56:121-132.

Sheridan, M.F. and J.R. Marshall, 1983. Interpretation of pyroclast surface features using SEM images. *Journal of Volcanological and Geothermal Research* 16:153-159.

Sheridan, M.F. and K. Wohletz, 1983. Hydrovolcanism: basic considerations and review. *Journal of Volcanological and Geothermal Research* 17:1-29.

Sigurdsson, H. and S. Carey, 1989. Plinian and co-ignimbrite tephra fall from the 1815 eruption of Tambora volcano. *Bulletin of Volcanology* 51: 243-270.

Sparks, R.S.J., H. Sigurdsson and L. Wilson, 1977. Magma mixing: a mechanism for triggering acid explosive eruptions. *Nature* 267:315-318.

Stern, C.R., 1991. Mid-Holocene tephra on Tierra del Fuego (54S) derived from the Hudson volcano (46S): evidence for a large explosive eruption. *Revista Geológica de Chile* 18:139-146.

Walker, G.P.L., 1981. Plinian eruptions and their deposits. *Bulletin of Volcanology* 44:223-240.

Wohletz, K., 1983. Mechanisms of hydrovolcanic pyroclast formation: grain-size, scanning electron microscopy, and experimental studies. *Journal of Volcanological and Geothermal Research* 17:31-63.

Wohletz, K., 1986. Explosive magma-water interactions: Thermodynamics, explosion mechanisms and field studies. *Bulletin of Volcanology* 48:245-264.

Zhang, Y., 1999. A criterion for the fragmentation of bubbly magma based on brittle failure theory. *Nature* 402: 648-650.

Zimanowski, B., R. Büttner, V. Lorenz and H.G. Häfele, 1997. Fragmentation of basaltic melt in the course of explosion volcanism. *Journal of Geophysical Research* 102:803-814.

Recibido: 07 de marzo de 2005
Aceptado: 20 de julio de 2005